# MICRO-ABRASION PACKAGE CAPTURE CELL EXPERIMENT ON THE TRAILING EDGE OF LDEF : IMPACTOR CHEMISTRY AND WHIPPLE BUMPER SHIELD EFFICIENCIES

Howard J. Fitzgerald and Hajime Yano
Unit for Space Sciences,
Physics Laboratory, University of Kent
Canterbury, Kent CT2 7NR
United Kingdom
Phone: +44-227-764000 ext. 7769, Fax: +44-227-762616

## SUMMARY

Four of the eight available double layer microparticle capture cells, flown as the experiment AO023 on the trailing (West) face of LDEF (Fig. 1), have been extensively studied. An investigation of the chemistry of impactors has been made using SEM/EDX techniques and the effectiveness of the capture cells as bumper shields has also been examined. Studies of these capture cells gave positive EDX results, with 53% of impact sites indicating the presence of some chemical residues, the predominant residue identified as being silicon in varying quantities.

## INTRODUCTION

An exposed area of 0.062 $m^2$ of both aluminium (Al) and brass foils, ranging in thickness from 1.5 $\mu$m to 24.13 $\mu$m were examined for hypervelocity perforations (Fig. 2). This initial examination concentrated on perforations in the top and bottom layers only. A total of 47 hypervelocity impact penetrations on the top layers have been found so far and their chemistry has been examined using a Philips 525M Scanning Electron Microscope (SEM) and Energy Dispersive X-ray (EDX) Spectroscopy techniques. Of these, 25 were found to have residues present but in 21 cases, this residue was silicon (Si) in varying abundance. Using a signal to background noise criteria, these were classified as Si-rich or Si-poor.

A natural impactor was identified on one of the top Al foils and one each of natural, man-made and Al-Si impactors were identified on the top brass layer. In addition, 10 perforations occurred in the second layer of a brass capture cell, each having Al residues and all due to a single large impact on the top brass layer. Around the surrounding areas of the secondary perforations, large numbers of craters were also seen. Also found were plasma perforations in 1.5 $\mu$m foil due to vaporised glue (ref. 1) which indicated Si residues but were not in fact hypervelocity in nature.

## CAPTURE CELL ARRANGEMENT

The principle behind the double layer capture cell is the use of a top foil as a "bumper shield" in order to dissociate hypervelocity impacting particles, and a second foil used as a "catcher" of impactor

residues (Fig 3). Chemical analysis via EDX techniques can then be employed to identify the source of these impactors from these residues.

The capture cells used consisted of triangular sections, with combinations of Al (T6 rolled Al of 99.9 % purity) and brass foils of varying thickness. The top and bottom layers were separated by 2.7 mm except in the case of the W8 section which had a separation of 14 mm. The cells occupied one third of an LDEF experimental tray and were arranged in two groups of 4 with a polished stop plate beneath the bottom layer. This initial investigation concentrated on the chemistry of perforations in both top and bottom layers. Further work remains to be done on matching up top perforations with their residues on the second layer as shown in Figure 4 (a)-(b).
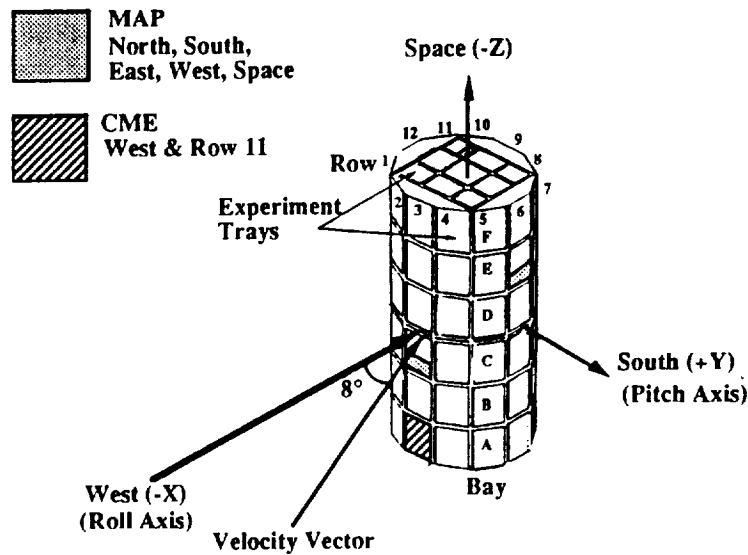


Figure 1. LDEF showing the positions of both the MAP and the CME experiments on the trailing edge.
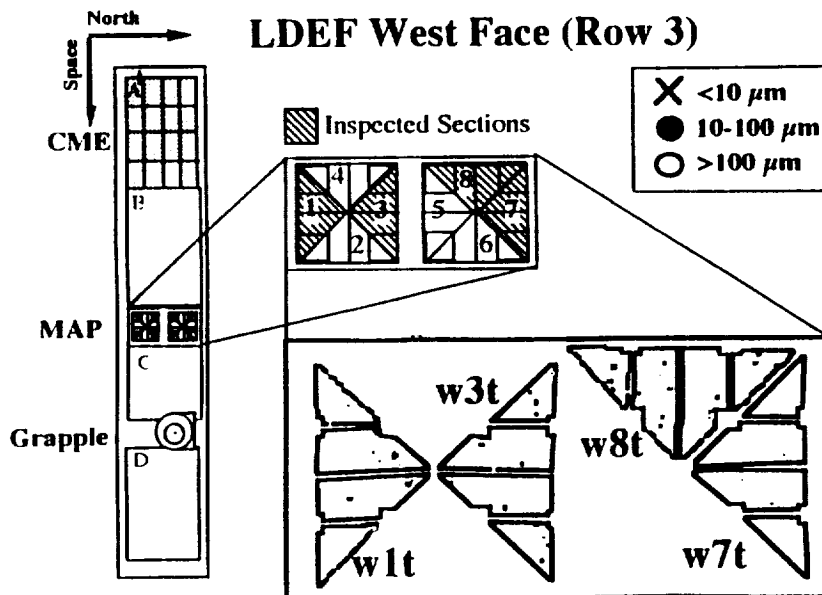


Figure 2. Arrangement of the west MAP foils on the experiment tray highlighting the sections inspected and the number and distribution of perforating impacts grouped into three size ranges.
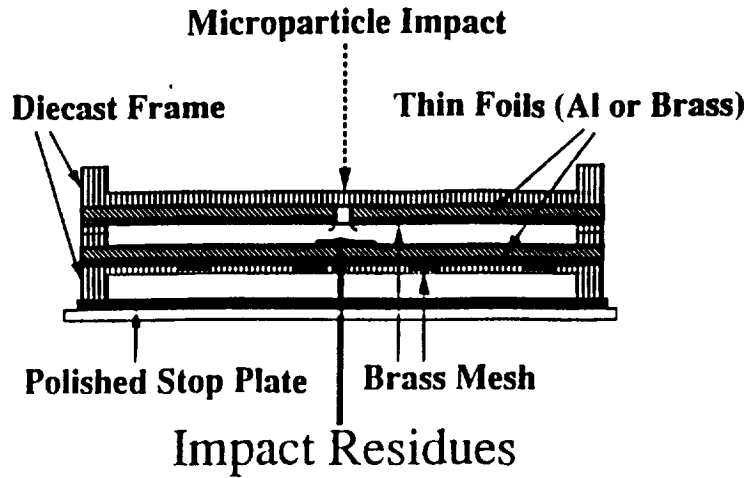
446

**Microparticle Impact**

**Diecast Frame**　　　　　　**Thin Foils (Al or Brass)**

**Polished Stop Plate**　|　**Brass Mesh**

# Impact Residues

Figure 3. Cross-sectional view of the Micro-Abrasion Package double layer capture cell

Y (mm)　Capture Cell Matching Impact Perforation (w8t/b)

X (mm)

Y (mm)　Secondary Perforation on the Bottom Layer by Debris Impact

Top 100 µm Penetration

Top Layer
(5 µm Brass)

Bottom Layer
(5 µm Brass)

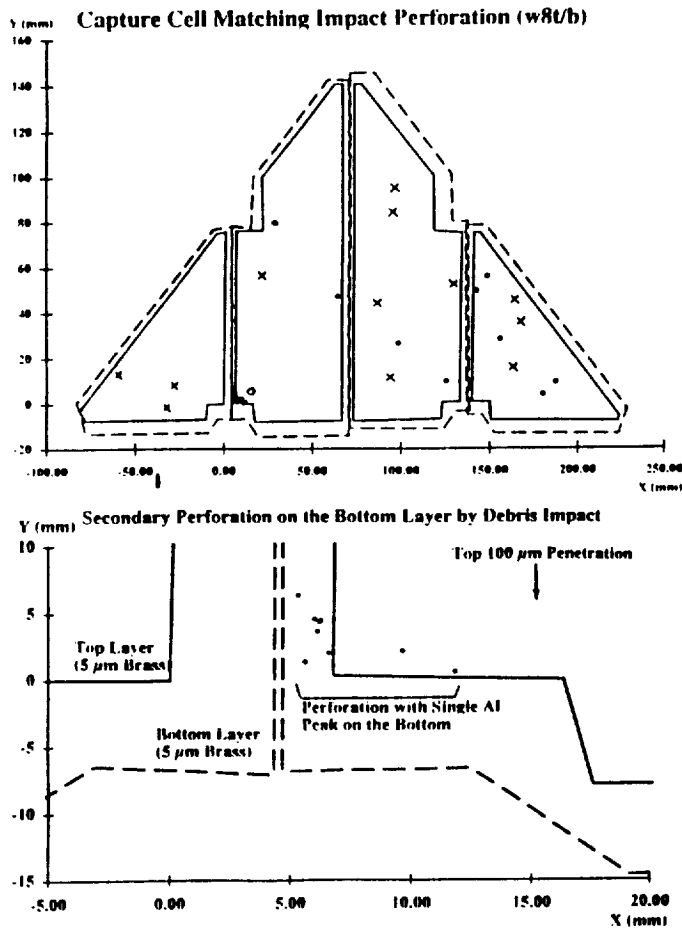Perforation with Single Al
Peak on the Bottom

X (mm)

Figure 4 (a)-(b). The two layers (a) of the W8 capture cell are overlaid with the bottom layer shown as dashed lines. Fig. 4b shows a close-up view of the region where 10 secondary perforations occurred in the second layer due to a 100µm impact in the top layer (shown here as a circle). Some of these perforations are very close and so appear to overlap in the diagram but all indicated single Al peaks suggesting the space debris origin.

# ANALYTICAL TECHNIQUE

All complete foil sections were first scanned using an automated stereo image CCD camera system called the Large Optical Scanning System (LOSS), for perforations by back illuminating the foils in a class 100 clean room (ref. 2). The penetration diameter size is derived from the CCD pixel count by fitting a photometric calibration curve, using holes which have been measured in the SEM. Initial scanning is at x10 magnification and potential impact sites are revisited at a variety of magnifications up to x40 with a resolution of > 4 μm. This enables most of obvious tears or rips to be distinguished from perforations which are due to actual space impacts.

Next, the foil sections were cut into their a, b, c, and d segments and placed in aluminium sample holders. The perforations were re-located using the co-ordinates derived from the optical scan and each feature was examined for morphology (ref. 3) and size using the SEM at a voltage of 25 kV and 0° tilt from normal. Actual hypervelocity impact sites were then imaged over a voltage range of 8-10 kV and an image taken at both 0° and 30° tilt.

Once a site had been identified as a hypervelocity event, a sequence of 6 X-ray spectra were taken with the EDX using a voltage of 20 kV and a count time of 100 seconds, with the stage tilted at 30°. This consisted of taking one spectrum of the entire site at a low magnification (which would indicate if large amounts of residue were present) followed by splitting the site into quadrants and examining a portion of the lip at high magnification. Finally, an X-ray spectrum of the nearby undamaged foil is taken, some 100-1000's of μm away from the impact site. The purpose of this was to provide a background spectrum for later use. The value for the count time of 100 seconds was chosen as a compromise value between the sensitivity of the instrument and the time available for investigation.

# CHEMICAL RESULTS

Of the 47 hypervelocity impacts examined, 53 % (Fig. 5-6) had identifiable residues. A total of 2 naturals, 1 man-made and 1 Al-Si impactors were positively identified. Figures 7 (a)-(c) show three hypervelocity perforations onto 24.13 μm Al foil and an example of a typical X-ray spectrum (d) indicated only silicon in varying quantities. In Figures 8 (a) and (b), the spectrum for the Al-Si impactor and an image of one of the 10 secondary perforations found in the second layer of a 5.0 μm capture cell are shown. An Al and Ni spectra was also indicated from residues on the bottom layer. The spectrum of Figure 9 (a) was obtained from an impact onto a 1.5 μm Al foil and shows peaks for Si and Mg as well as S and was classified as due to a natural particle. The Cl may be due to contamination. The Figure 9 (b) was obtained on a 5.0 μm brass foil and displays strong peaks for Ca, Si, Al and Mg and it was also due to a natural particle. A solid line in the figures indicates a background spectrum.

Only the top layer of the capture cells (except for w8bb) were examined and despite the fact that EDX was performed only on the lips, the results compare well with the Chemistry of Micrometeoroid Experiment (CME, AO187-1) equipped with thick gold (Au) plate target on the same west face of the LDEF (ref. 4-5), where less than 50 % of impact sites had identifiable residues. The bottom layers may have substantial quantities of intact or semi-intact materials which could lead to further identification of unknowns as well as explaining the prevalence of Si residues. It is also noted that there can be different

C-4

elemental measurements at different locations (e.g. lip, bottom, side wall) within one hemispherical impact crater due to non-homogeneity of composition of an impactor (ref. 6).
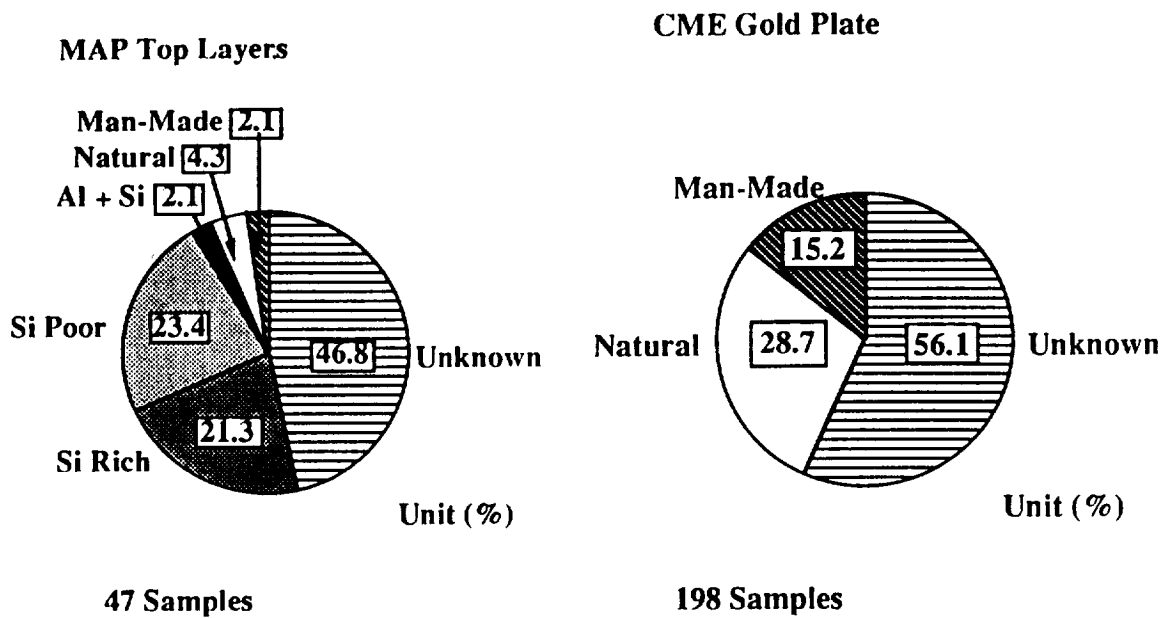
**MAP Top Layers**

**CME Gold Plate**



47 Samples

198 Samples

Figure 5. Chemical results of the MAP data comparing to the CME data



Outer: Aluminium (25)
Inner: Brass (22)

Signal / Background (σ)
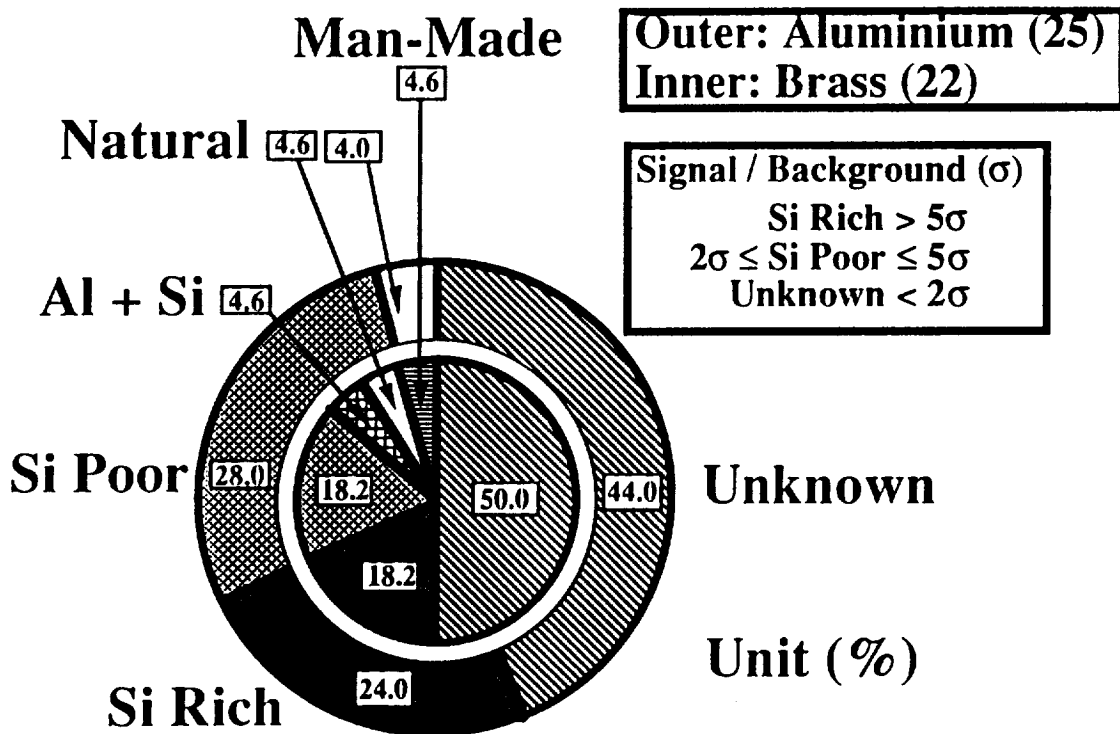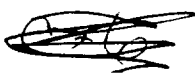Si Rich > 5σ
2σ ≤ Si Poor ≤ 5σ
Unknown < 2σ

Figure 6. Breakdown distribution of impactors onto respective Al and Brass foils of the west MAP

## INTERPRETATION OF THE CHEMISTRY

The majority of hypervelocity impacts with detectable residues were classed as either Si-rich or Si-poor, since the only residue detected was that of silicon. The interpretation of the two sub-groups was made by the following criteria. The Si peak of the best lip spectra was compared to the silicon peak of the background, initially comparing the count rates of these peaks. The Signal/Noise (S/N) was interpreted as the ratio of the two counts. (1) if $S/N < 2$, chemistry classed as unknown; (2) if $2 \leq S/N \leq 5$, chemistry classed as Si-poor; and (3) if $S/N > 5$, chemistry classed as Si-rich.

Then a background subtraction routine was applied to both lip and background spectra. The peak count rates were again compared to verify the first results. A better way of finding the S/N ratio would be to compare the areas under each of the respective peaks. However, the method used was found to be a good approximation to this. The spectra identified as man-made, natural or Al-Si had clear peaks and presented no problem in identification.

## FLUX MEASUREMENTS

The experimental data for the flux on the trailing edge of LDEF was in good agreement to previously obtained results, using a variety of sources such as the LDEF intercostals and clamps, which has been combined into a plot known as the west face smooth data (ref. 7). The data shows particularly good agreement at the smaller marginal perforation limit (Fmarg) but diverges from the smoothed curve in the other cases. This can probably be explained as being due to the small sample sizes available for each different thickness (Fig. 10).

The 5.0 μm brass data was initially converted into an equivalent thickness of aluminium by inputting appropriate values of density and tensile strength into the CMD equation for both Al and brass, which resulted that Brass : Al = 1.88 : 1(ref. 7-9). However, this is a rather crude way of equating the two materials and the data was plotted as brass instead. It shows good agreement with the West smoothed plot but diverges at higher marginal perforation values. In order to derive the marginal penetration value (Fmarg) from the experimental values of perforation size (Dh), it was first necessary to normalise the diameter of each hole to some average value, since the majority of perforations were elliptical in nature.

A computer generated program (ref. 11) was then employed to output values of Fmarg and diameter of impacting particle using the CMD equation. The assumption was made that all impactors were natural, with a normal impact velocity of 11.01 km/s and density of 1.00 g/cm$^3$, since the program did not allow for a combination of natural and man-made debris to be calculated.

## COMPARISON OF MAP DATA WITH CDC AND CME RESULTS

The perforation sizes for the MAP data has been converted into particle size using the equation derived by Cour-Palais (ref. 12) in order to make a direct comparison to data from both the Cosmic Dust Catalogue (CDC) (ref. 13) and the CME (ref. 14). CDC data represents micrometeoroid particles that
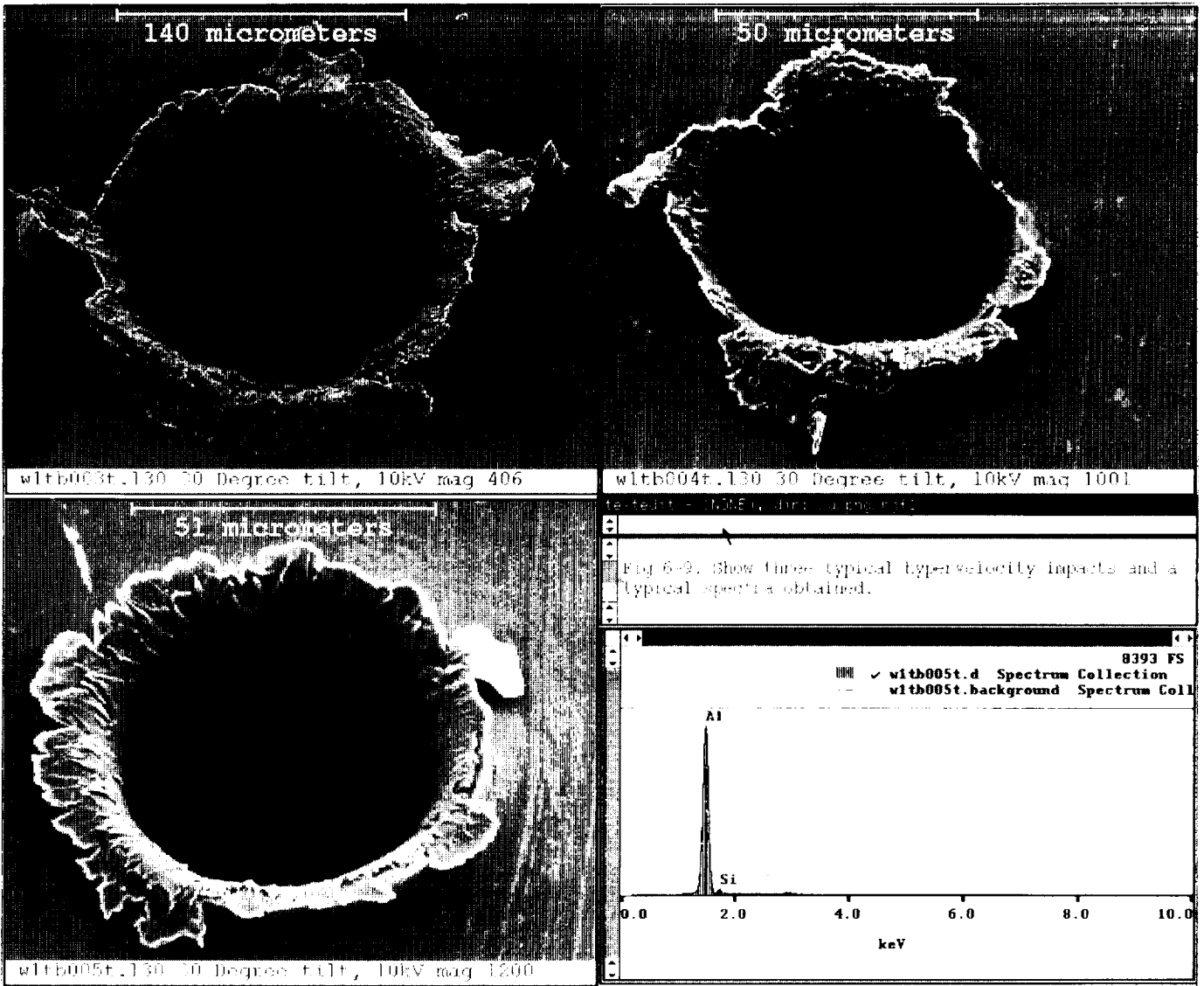
Figure 7 (a)-(d). Three hypervelocity perforations onto 24.13 µm Al foils (a)-(c) and a typical X-ray spectrum (d = bottom right)
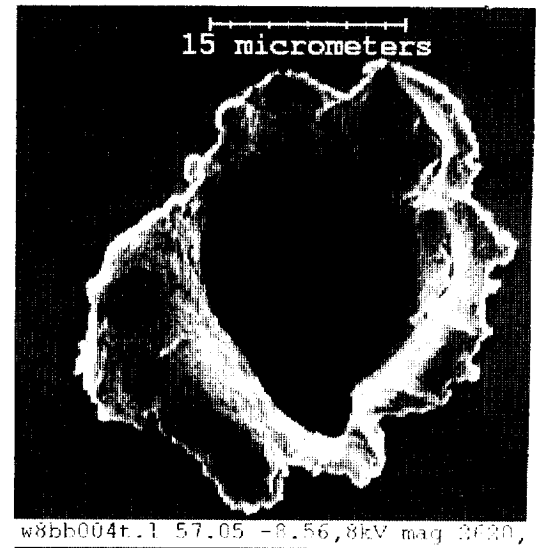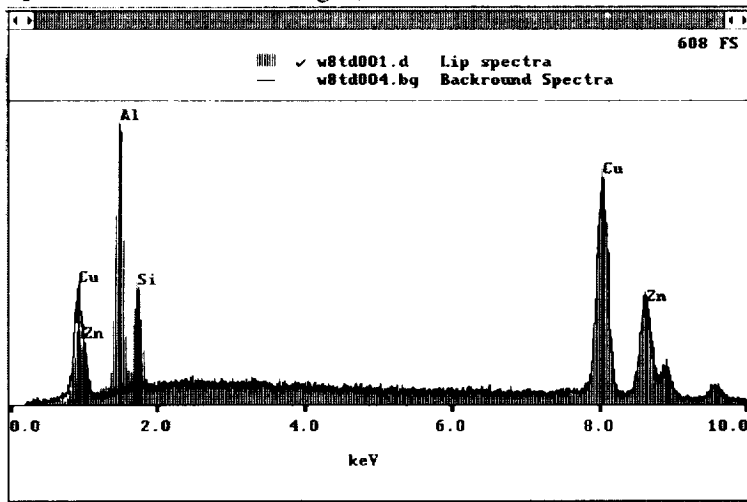


Figure 8 (a)-(b). Spectrum for Al-Si impactor (a = left) and an image of one of 10 bottom perforations on 5 µm capture cell (b = right).
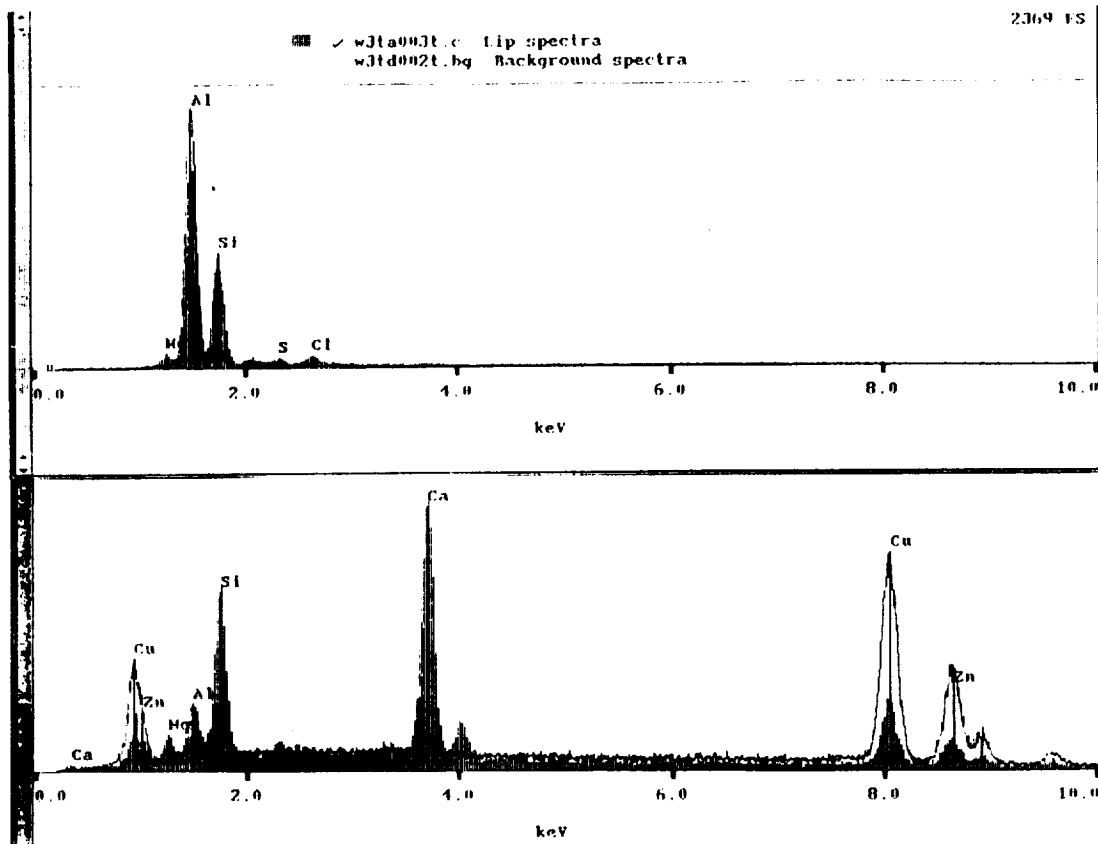
Figure 9 (a)-(b). The spectrum (a = top) was obtained from an impact onto a 1.5 μm Al foil with Si, Mg, and S peaks due to a natural particle. The Cl peak may be due to contamination. The spectrum (b = bottom) was obtained on a 5.0 μm brass foil displaying strong Ca, Si, Al, and Mg peaks also due to a natural particle.
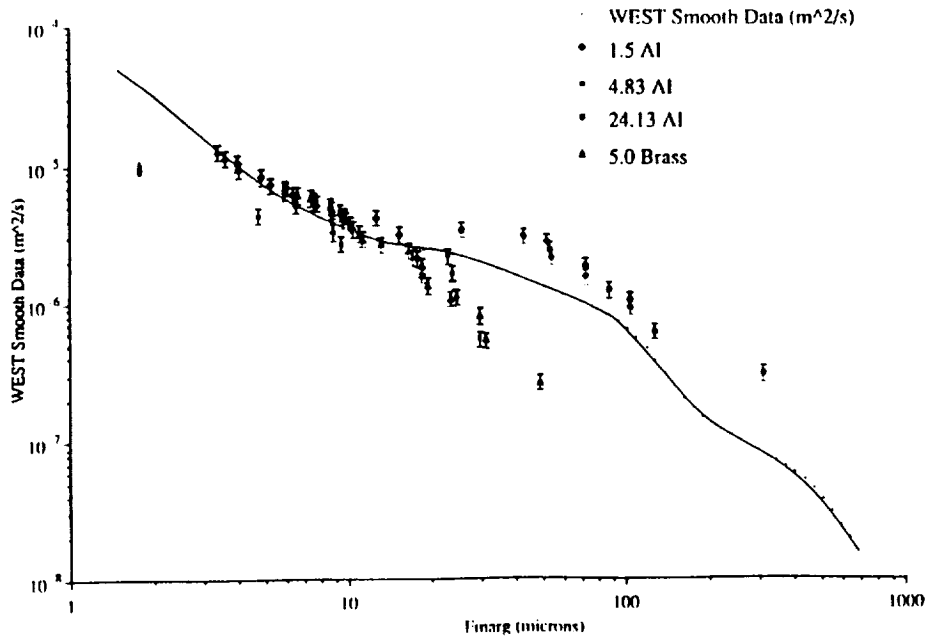
WEST Smooth Data (m^2/s)
• 1.5 Al
• 4.83 Al
• 24.13 Al
▲ 5.0 Brass

Figure 10. Experimental flux for MAP west foils against a smoothed curve of the same face of LDEF

452

The trend of MAP unknown particles follows that of CME unknowns and CDC natural particles (Fig. 11). All the CME unknowns are assumed to be caused by natural particle impacts with much higher impact velocities than catching-up debris from the trailing direction of the LDEF. However, higher peaks of Si particles occur in the size range 3-6 μm. These could be due to the larger than previously anticipated Si debris in the LEO. Limitation of CDC data is that detection range is only 3-50 μm and for CME, the use of a semi-infinite target means that it is insensitive to small impactors.
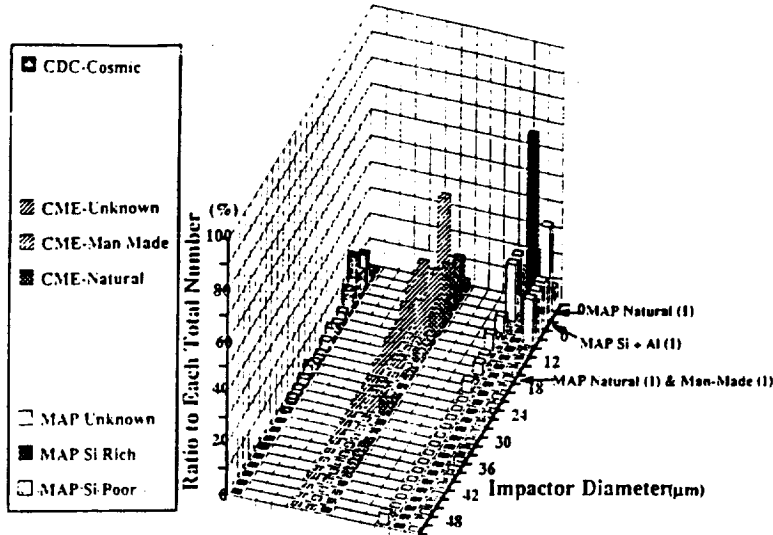


Figure 11. The impactor size distribution for CDC, CME and MAP West data

## BUMPER SHIELD EFFICIENCIES

The effectiveness of the capture cells in terms of bumper shields (ref. 15) was investigated by converting the two layer foil thickness into an equivalent single thickness and plotting the thickness of foil that would be just perforated (the marginal perforation limit: Fmarg) against the cumulative flux, using the smoothed data curve.

| Segment | Material | Thickness (microns) Top/bottom | Area (cm^2) |
|---|---|---|---|
| w1ta/d | Br | 5.0 Br / 12.0 Br | 52.54 |
| w1tb/c | Al | 24.13 Al / 12.0 Br | 101.75 |
| w3ta/d | Al | 1.5 Al / 12.0 Br | 53.25 |
| w3tb/c | Al | 4.83 Al / 12.0 Br | 101.75 |
| w7ta | Al | 12.13 Al / 4.90 Al | 26.73 |
| w7tb/d | Al | 24.13 Al / 4.90 Al | 78.86 |
| w7tc | Al | 14.11 Al/ 4.90 Al | 52.13 |
| w8ta-d | Br | 5.0 Br / 5.0 Br | 155 |

Table 1 : Lists material, exposed area and possible combinations of thickness of foils evaluated as bumper shields. Only combinations that had not had the 2nd layer penetrated were considered.

The value of flux that can be protected against for the single (equivalent) thickness can be read directly from the diagram (Fig. 12). If the actual flux to which the west capture cells were exposed is higher than this value, and the capture cells have prevented penetration of their second layer, then the efficiency of the bumper shield concept has been proven. Table 1 gives details of thickness and exposed area for the different segments of the capture cells. The analysis indicated however that only one out of four combinations of combined foil thickness of the west MAP capture cells was found to be more efficient than a single shield. This can be explained as being due to too short an exposure time.

However, it was found that a single 100µm impact onto the top 5.0 µm brass foil of the w8 capture cells caused 10 secondary perforations of the 2nd 5.0 µm brass foil, despite a separation of 14.7 mm between the two layers. This suggests that greater attention needs to be paid to the protection of vital components situated on the trailing edge of a spacecraft in LEO.

## W7 BUMPER EFFICIENCY



A : 14.11 Al + 4.90 Al = 19.01 µm Al
B : 24.13 Al + 4.90 Al = 29.03 µm Al
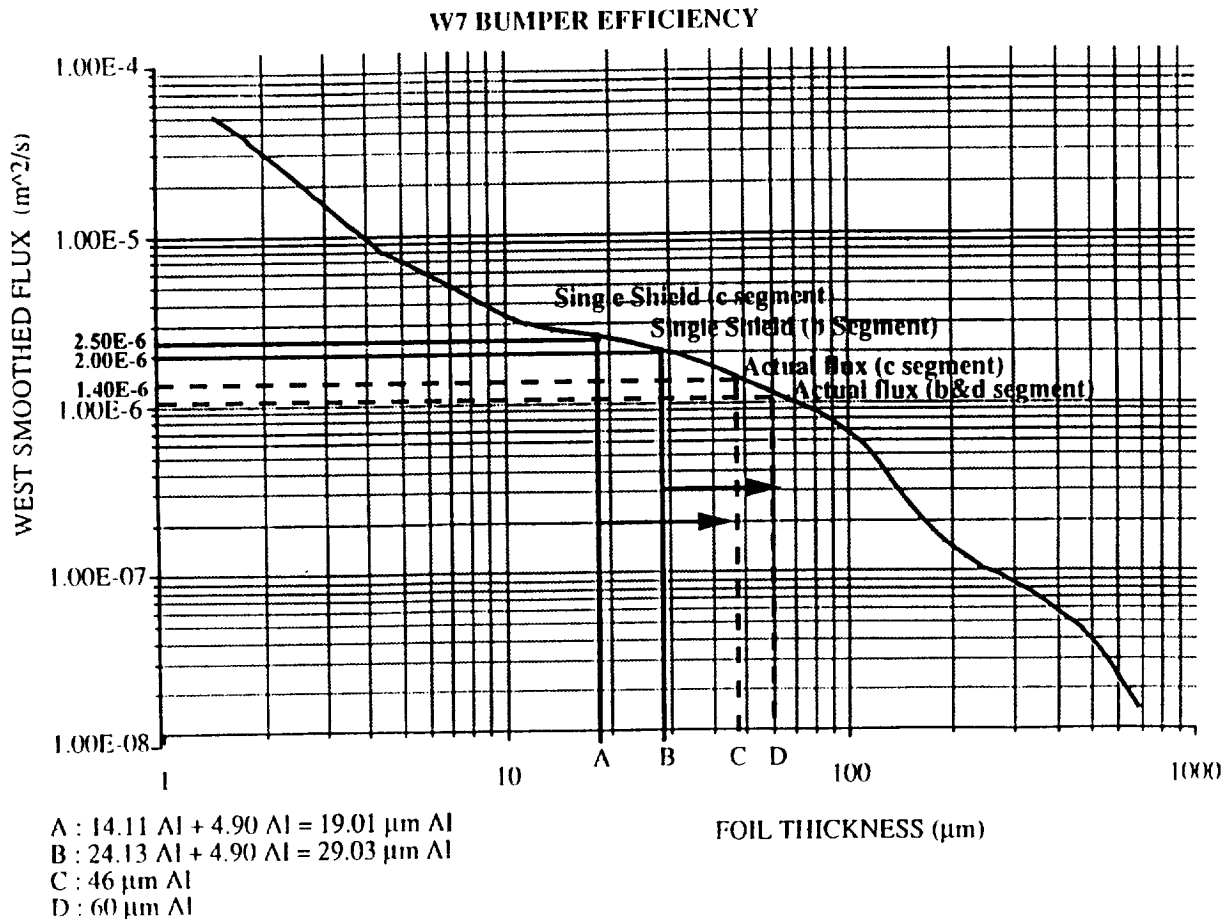C : 46 µm Al
D : 60 µm Al

FOIL THICKNESS (µm)

Figure 12. The bumper shield efficiency for the W7 brass foil. A = Sum of bumper shield thickness (14.11 µm Al + 4.90 µm Al), B = Sum of bumper shield thickness (24.13 µm Al + 4.90 µm Al), C = Single shield with equivalent shielding effect of bumper A (46 µm Al), and D = Single shield with equivalent shielding effect of bumper B (60 µm Al).

454

The speed at which a particle impacts the capture cell will largely determine the degree of vaporisation that the particle will undergo. Despite the fact that the capture cells were situated on the trailing edge, it is still possible that natural particles can strike the spacecraft at up to ~70 km/s. In the case of space debris, the maximum normal, relative impact velocity is 3.16 km/s, which implies that there would be a greater chance of detecting man-made debris compared to natural particulate. Major sources of man-made debris are aluminium parts of spacecraft and solidified $Al_2O_3$ rocket propellant spheres. However, 2/3 of the top detector surface was in fact aluminium foil, thus rendering this area insensitive to the detection of those debris with conventional EDX technique. Impact events at speeds > 3 km/s subject both target material and impactor to extremes of temperature and pressure leading to fragmentation, melting or vaporisation (ref. 16) and the most important material parameters for both target and particle are density and the boiling point of the material.

It has been shown that the impact of a high density impactor onto a low density target will experience the least damage while conversely, a low density impactor onto a high density target will result in the most damage. The MAP experiment is an example of the former, where low density (Al) and medium density (brass) foils are used as the target material. The advantage of Al are the lower shock conditions and temperatures generated during the event. The drawback is that the foils are insensitive to the majority of the man-made particle population. Brass foils offer an intermediate detector surface between Al and Au as well as offering a characteristic spectrum which does not interfere with identification of extra-terrestrial materials. However, the 5.0 μm thickness used did prove to be insensitive to the smallest sized micrometeoroid. The CME experiment is an example of the latter, where a high density semi-infinite target material (Au) was used as the detector surface. The result of this is that hypervelocity impact events generate higher shock-stresses and temperatures resulting in a greater degree of vaporisation and subsequent non-detection of residues due to being below the sensitivity of EDX method employed.

In general, EDX analysis requires more than 1 % of the material being examined to be residue. Since in the case of the MAP foils, the major portion of the particle has passed through the top layer, the amount of residue present is close to this 1 % value. It is also possible that at times during the EDX examination, the X-ray beam was actually passing through the surface of lips, since these X-rays may typically penetrate up to 1 μm of material. An X-ray voltage of 3-5 kV has been suggested to overcome this problem and will be used in future analysis of residues on the second layer.

CONCLUSIONS

The effectiveness of the capture cell principle has been demonstrated over the use of higher density semi-infinite detectors. Preliminary results have shown that EDX techniques can be employed successfully in the analysis and identification of residues and compare well with previous studies on the CME.

Note has been taken of comments raised during the conference, namely that lower X-ray voltages, of the order of 5 kV may increase the success rate of EDX analysis. Use of a voltage of 20 kV has probably resulted in the electron beam passing through the residue in some cases. This suggestion will be incorporated in future studies of the second layer. Also noted is the fact that there may be more silicon

debris than earlier anticipated. If this is the case, then the detection of the large number of Si impactors can be explained. In terms of contamination of the foils, Mg-Si pockets of impurities have been reported (ref. 17) but we do not believe this to be detrimental to our results, since only small portion (some 10 $\mu$m x 10 $\mu$m at most) of hypervelocity lips were examined and the fact that Mg has only been detected at a couple of sites reinforces this view.

Comparison of MAP data with CME and CDC has revealed the MAP foils detected a higher number of particles in the 2-5 $\mu$m size range. These particles were identified as Si-rich or Si-poor. This suggests that the population of small size particles is larger than previously estimated and may be due, in part at least, to man-made silicon debris. Overall, the data shows agreement with the trend of decreasing population with increasing particle diameter.

Flux measurements have shown good agreement with previous experimental data. Anomalies and divergence from the smoothed data curve can be explained by the small statistics involved. Additional data has been measured for the lower marginal perforation limit (1.5 $\mu$m) and the data shows excellent agreement with the smoothed data. The effectiveness of the capture cells as bumper shields has also been examined with the real space data. However, in the exposure time of the LDEF (5.78 years), their have been insufficient impacts on the trailing edge to prove the efficiency of the MAP structure as a bumper shield.

## ACKNOWLEDGEMENTS

## REFERENCES

1. Yano, H. and Fitzgerald, H.J., Determination of directionality and sources of impactors on the double layer foil capture cells of LDEF, *Proc. First European Conf. on Space Debris*, ESA SD-01, 207-210, (1993).

2. Paley, M.T., An automated system for obtaining impact penetration, location, size and circularity on a foil with special reference to the LDEF, *Hypervelocity Impacts in Space*, J.A.M. McDonnell (Edit), University of Kent at Canterbury, Kent, UK, 48-53, (1992).

3. Mackay, N.G., Green, S.F., Deshpande, S.P. and Newman, P.J., Interpretation of impact crater morphology and residues on LDEF using 3-D space debris and micrometeoroid models, *Proc. First European Conf. on Space Debris*, ESA SD-01, 159-164, (1993).

4. Hörz, F., Bernhard, R.P., Warren, J.L., See, T.H., Brownlee, D.E., Laurance, M.R., Messenger, S., and Peterson, R.B., Preliminary analysis of LDEF instrument AO187-1 "Chemistry of Micrometeoroids Experiment", *Proc. First LDEF Post-Retrieval Symp.*, NASA CP-3134, 487-501 (1992).

5. Hörz, F. and Bernhard, R.P., Compositional Analysis and Classification of Projectile Residues in LDEF Impact Craters, NASA Tech. Memo. 104750, NASA/JSC, Houston, USA (1992).

6. Berthoud, L. and Mandeville, J.C., Further analysis of remnants found in LDEF and MIR impact craters, Presented at the Workshop on Interplanetary Dust Particles, Houston, TX, USA, May, 1993.

7. Neish, M.J., In-house communication, (1993).

8. Deshpande, S.P. and Paley, M.T., Supra-marginal impacts detected on the Micro-Abrasion Package (MAP) experiment situated on LDEF's space face, Hypervelocity Impacts in Space, J.A.M. McDonnell (Edit), University of Kent at Canterbury, Kent, UK, 166-172, (1992).

9. McDonnell, J.A.M., Deshpande, S.P., Niblett, D.H., Neish, M.J., and Newman, P.J., The near Earth space environment - an LDEF overview -, *Adv. Space Res.*, 13, 8, (1993).

10. Berthoud, L. and Mandeville, J.C., Empirical impact equations and marginal perforation, Proc. First European Conf. on Space Debris, ESA SD-01, 459-464, (1993).

11. Deshpande, S.P., In-house communication, (1993).

12. Cour-Palais, B.G., Hypervelocity impacts in metals, glass, and composites, *Int. J. Impact Eng.*, 5, 681-692, (1987).

13. NASA Cosmic Dust Preliminary Examination Team (M. Zolensky et.al.), Vol. 1-13, NASA Johnson Space Center, Houston, Texas, USA, (1982-1992).

14. Yano, H., Comparative studies of chemical components of impact residues on the LDEF, stratospheric particles and Antarctic ice core particles, *Annal. Geophys.*, Part 3, 11, C481, (1993).

15. Whipple, F.L., Meteorites and space travel, *Astron. J.*, 52, p.5, (1947).

16. Yano, H., Fitzgerald, H.J., and McDonnell, J.A.M., Chemical analysis of natural particulate impacts on the Long Duration Exposure Facility, Presented at the IAU Symposium 160 : Asteroids, Comets, Meteors 1993, Belgirate, Italy, June 1993.

17. Berthoud, L., In-house communication, (1993).